Journal of Fluids and Structures 85 (2019) 17–26

Contents lists available at ScienceDirect

Journal of Fluids and Structures

journal homepage: www.elsevier.com/locate/jfs

A wind tunnel study of wind loads on a model wind turbine in atmospheric boundary layer winds

Wei Tian [a,b], Ahmet Ozbay [b], Hui Hu [b,*]

[a] School of Aeronautics and Astronautics, Shanghai Jiao Tong University, Shanghai, 200240, China
[b] Department of Aerospace Engineering, Iowa State University, Ames, IA, 50010, United States

ARTICLE INFO

Article history:
Received 5 March 2018
Received in revised form 2 December 2018
Accepted 4 December 2018
Available online 14 December 2018

Keywords:
Wind turbine aerodynamics
Dynamic wind loads
Atmospheric boundary layer (ABL) wind
Wind tunnel

ABSTRACT

A wind tunnel study was conducted to investigate the dynamic wind loads that act on a model wind turbine placed in an atmospheric boundary layer wind tunnel. Two types of atmospheric boundary layer winds with neutral conditions were simulated to quantify the influences of wind shear and turbulence intensity on the dynamic wind loads of the model wind turbine as it operated at different tip-speed-ratios. While the wind shear was recognized as an important factor for the mean wind loads, the turbulence intensity dominated the behavior of the fatigue loads that acted on the model wind turbine. A further investigation of the wind loads acting on different components of the model wind turbine revealed that more than 90% of both the mean and fatigue wind loads were contributed by the rotating rotor of the wind turbine. The mean wind loads on a stationary wind turbine can be as high as approximately 38% of the mean wind loads that act on a rotating wind turbine. By changing the blade phase angle of a stationary wind turbine model, the maximum variation of the mean wind loads was found to be 15%, while fatigue loads vary by 10%.

1. Introduction

The mechanical design of a wind turbine structure is affected by the mean loading and fatigue loading, which are difficult to characterize because they have variable amplitudes, and the intensity of the variations depends on the environmental wind climate. To conduct effective wind load analysis, the factors that affect the dynamic wind loads acting on a wind turbine must be comprehensively considered. These factors include wake induced effects (Larsen et al., 2013), terrain characteristics (Riziotis and Voutsinas, 2000), extreme wind conditions, such as thunderstorms (Nguyen and Manuel, 2015) and downbursts (Zhang et al., 2015), and the characteristics of atmospheric boundary layer (ABL) winds, such as wind shear (Dimitrov et al., 2015) and thermal stability (Sathe et al., 2013). Dimitrov et al. (2017) and Abdallah et al. (2016) indicated that fatigue damage to wind turbines is mainly caused by stochastic loading due to turbulence. Modern wind turbines operate under many different terrain conditions, ranging from relatively flat sites, such as offshore environments with relatively low turbulence, to complex terrain with high turbulence. However, how the wind turbine performs under these conditions is often unclear.

Time series of wind turbine loading are usually obtained from prototype measurements (Bak et al., 2013; Barthelmie et al., 2005; Yoshida et al., 2016). These measurements are carried out with test sites that often feature benign climatic conditions. However, because the flow conditions cannot be controlled in onsite tests, it is difficult to use these measurements to accurately predict the fatigue loads on a wind turbine at a particular site. In addition to full-scale field measurements, several

* Corresponding author.
E-mail address: huhui@iastate.edu (H. Hu).

https://doi.org/10.1016/j.jfluidstructs.2018.12.003
0889-9746/

numerical modeling approaches have been implemented to predict the dynamic responses of wind turbines. Moriarty et al. (2004) generated multiple samples of loading data under various wind conditions using a stochastic turbulence simulator coupled with the aeroelastic code. Furthermore, Lee et al. (2011) investigated the atmospheric and wake turbulence impacts on wind turbines using a two-way coupled aeroelastic tool with large eddy simulation (LES). Dimitrov (2015) tested the performance of statistical extrapolation methods in predicting the extreme load response of a multi-megawatt wind turbine. Although researchers have developed different models to predict the behaviors of wind loads, there is still space for using present developed simulations to accurately predict the dynamic loads that act on wind turbine under different conditions. One challenge associated with the development of these numerical models is the lack of quantitative experimental and field measurement data to verify the numerical simulation results.

Wind tunnel facilities have been widely used for model wind turbine studies due to their ability to produce well-controlled flow environments. Hu et al. (2012) conducted an experimental study on a wind turbine model and found that the instantaneous wind loads that act on the model wind turbine are highly unsteady and have randomly fluctuating magnitudes, which can be 2–3 times higher than the time-averaged values. Recently, Jiang et al. (2015) performed a long-term fatigue analysis of rolling element bearings in wind turbine gearboxes using the loads of the National Renewable Energy Laboratory's (NREL) 750 kW wind turbine. The characteristics of wind loads shown by Hu et al. (2012) via conducting wind tunnel testing are found to be quite similar to the results provided by Jiang et al. (2015).

In general, due to the limit of wind tunnel size, the Reynolds number of a large, utility-scale wind turbine operating in atmospheric flow cannot be matched by wind-tunnel experiments. The Reynolds number of utility-scale wind turbine is typically in the range of 0.7×10^6 to 10×10^6 (Wilson, 1994), which is 2–3 orders of magnitude higher than that can be simulated in wind tunnel testing. According to the studies conducted by Alfredsson et al. (1982), Whale et al. (2000) and Medici and Alfredsson (2006), due to the fact that the boundary layer flow over wind turbine blades is highly sensitive to Reynolds numbers, such a low Reynolds number may affect the aeromechanic performances of the wind turbine greatly. For example, the maximum power output and thrust coefficients could be lower for a small-scale model turbine operating at a lower Reynolds number. However, Vermeer et al. (2003), Grant et al. (1997), Haans et al. (2008) and Adaramola and Krogstad (2011) indicated that, in test cases for comparison with and validation of numerical models, the testing results at a lower Reynolds number are acceptable as long as the aerodynamic characteristics of the rotor blades are known in the modeled Reynolds number range. Therefore, quantitative measurements of wind tunnel studies under low Reynolds number conditions can be used as a database to validate and verify numerical simulations.

While extensive experimental studies have been performed previously to characterize the power generation and aerodynamic performances of wind turbines, very little can be found in literature for the wind tunnel studies to specifically evaluate the effects of ABL inflow characteristics on the dynamic wind loads acting on wind turbines. With this in mind, by generating two types of ABL surface winds in a large-scale ABL wind tunnel, we firstly conducted a comprehensive experimental study to investigate the effects of wind shear and turbulence intensity levels in the incoming ABL winds on the dynamic wind loads acting on a wind turbine model. Then, by disassembling the wind turbine model into different parts, a further experimental study was performed to characterize the contributions of each components of the model wind turbine (i.e., tower, nacelle and rotor) to the total wind loads acting on the turbine model. Finally, the characteristics of the dynamic wind loads acting on a wind turbine were also studied with the model wind turbine being set in "shut-down" mode, i.e., the scenario when the incoming wind speeds exceed the typical "cut-out" speed of wind turbines (i.e., >25 m/s). The optimal phase angles to place the turbine rotor blades were identified in order to shut down a wind turbine when the incoming airflow exceeds the "cut-out" speed. It should be noted that, while a preliminary version of the work was previously reported in a conference paper (Tian et al., 2014a), considerable new measurement results and more comprehensive discussions/analysis about the measurement results have been added in the present study to elucidate the underlying physics to gain further insight into the characteristics of dynamic wind loads acting on wind turbines when operating in atmospheric boundary layer winds.

2. Experimental setup

The experiments were conducted in a large-scale aerodynamic/atmospheric boundary layer (AABL) wind tunnel located at the Aerospace Engineering Department of Iowa State University. The AABL wind tunnel is a closed circuit wind tunnel with a test section that is 20 m long, 2.4 m wide and 2.3 m high. As shown in Fig. 1, five equally distributed triangular spires and a wooden plate were mounted at the inlet of the test section in order to generate ABL winds with desired mean shear profiles at the measurement locations. In the present study, the spires with aspect ratios of 0.12 and 0.16 were used to generate two types of ABL winds with different velocity gradients and turbulence intensity levels. The wooden plate mounted on the wind tunnel floor to connect to the five spires is 200 mm in height. In addition, surface roughness elements (i.e., wooden blocks) with different size and spacing were also mounted on the wind tunnel floor to generate different levels of turbulence intensity for the ABL winds. By using different combinations of the roughness elements and triangle shaped spires, different types of fully developed neutrally-stratified ABL winds with distinct mean and turbulence characteristics can be generated in the AABL wind tunnel. The growth of the boundary layer of the simulated ABL wind under zero pressure gradient conditions was achieved by adjusting the ceiling profile of the test section of the wind tunnel.

Fig. 1. The test section of the AABL wind tunnel.

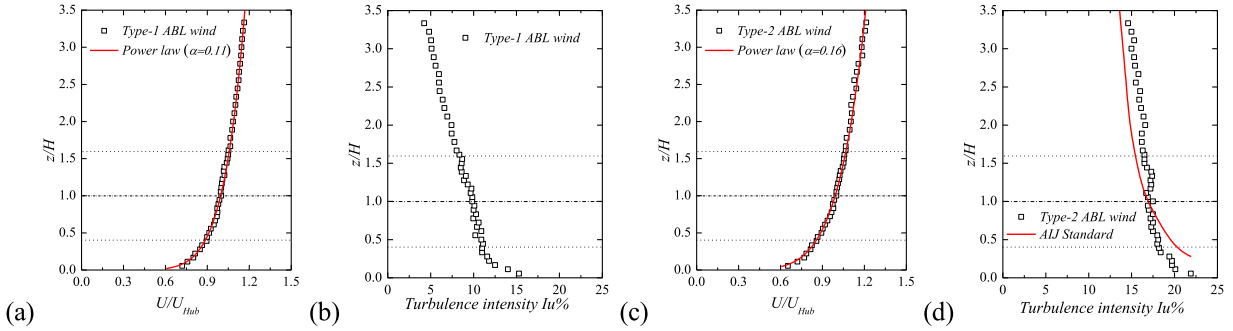

Fig. 2. Characteristics of the simulated ABL winds under neutral conditions. (a) type-1 ABL wind, stream-wise mean velocity; (b) type-1 ABL wind, turbulence intensity; (c) type-2 ABL wind, stream-wise mean velocity; (d) type-2 ABL wind, turbulence intensity. The two dotted lines represent the top and bottom tip heights of the wind turbine, and the dash-dotted line represents the hub height.

Wind shear is often defined using a simple exponential law (IEC, 2005), which defines the mean wind speed U at a height z above ground using the wind speed U_{Hub} that is measured at a turbine hub height H as a reference:

$$\frac{U}{U_{Hub}} = \left(\frac{z}{H}\right)^{\alpha} \tag{1}$$

where α is a constant exponent. According to ASCE standard (Zhou and Kareem, 2002), different exponents can represent different types of open terrain. As shown in Fig. 2(a), the power-law exponent for the type-1 ABL wind is $\alpha = 0.11$, which can be used to represent offshore (open sea) terrain. The corresponding turbulence intensity shown in Fig. 2(b) was found to be approximately 9.5% at the hub height ($z/H = 1$), which is in the range of the turbulent ABL winds over the open sea based on the onsite measurements of Hansen et al. (2012) at the Horns Rev offshore wind farm. Here, the turbulence intensity is calculated by using the expression of $I_u = \sigma_u/Ulocal$, where σ_u is the root-mean-square of the turbulent velocity fluctuations, and U_{local} is the mean wind speed at the measurement point. The exponent for the type-2 ABL wind shown in Fig. 2(c) is $\alpha = 0.16$, which can be used to represent an onshore wind farm sited on open country terrain with low scrub or scattered trees. Fig. 2(d) shows the turbulence intensity as a function of the height above the floor of the AABL wind tunnel. The turbulence intensity is consistent with the standard turbulence intensity profile of an ABL wind over open terrain as suggested by the Architectural Institute of Japan (AIJ , 1996). It should be noted that, the turbulence intensity level at the turbine hub height for the type-2 ABL wind is approximately 18.0%, which is close to the turbulence intensity levels measured in an onshore wind farm as reported by Smith et al. (2013).

In the present study, a Cobra Probe anemometry system (Turbulent Flow Instrumentation Pty Ltd.) was applied to measure the instantaneous wind speeds of the ABL wind. By using the Cobra Probe, all three components of airflow velocity could be measured instantaneously. The mean velocity and turbulent intensity can also be calculated after obtaining the instantaneous measurement data. The sampling rate of the instantaneous velocity measurements was set to be 1250 Hz with a measurement period of 60 s at each point of interest.

The wind turbine model used for this study represents the most widely used three-blade horizontal axial wind turbines (HAWTs). The model wind turbine has a rotor radius of 140 mm, and the height of the turbine nacelle is 225 mm above the wind tunnel floor. With a scale ratio of 1:350, the test model would represent a wind turbine in a wind farm with a rotor diameter of approximately 90 m and a tower height of approximately 80 m. The blade of the tested model was generated based on the ERS-100 prototype of wind turbine blade developed by TPI. The blade has a constant circular cross section from

Table 1
Thrust coefficients of wind turbine models used in wind tunnel studies.

Wind tunnel studies	Hu et al. (2012)	Zhang et al. (2012)	Cal et al. (2010)	Hancock and Pascheke (2010)	The present study
Tip speed ratio,	3.0	3.7	4.9	6.05	6.0
Thrust coefficient, C_T	0.31	0.42	0.32	0.497	0.538

the blade root to 5% of the blade radius (R), and three NREL airfoil profiles (S819, S820, S821) are used at different span-wise locations along the rotor blade. The S821 airfoil profile is used between 0.208R and 0.40R, the S819 primary airfoil is positioned at 0.70R, and the S820 airfoil profile is located at 0.95R. Further information about the ERS-100 rotor blades are available at Locke and Valencia (2004) and Somers (2005). Furthermore, to analyze the dynamic wind loads acting on different components of the model wind turbine, the test model was disassembled into three parts: tower, nacelle and rotor. Additional details about the wind turbine model can be found in Tian et al. (2014b) and Yuan et al. (2014).

The angular velocity of the turbine blades was adjusted by applying different electric loads to a small DC motor (Kysan, FF-050S-07330) installed inside the turbine nacelle. The turbine angular velocity (i.e., Ω) can change from 0 to 2200 rpm and the corresponding tip-speed-ratio (i.e., $\lambda = \Omega\ (2\pi/60)R/U_{Hub}$, where R is the radius of the rotor) ranges from 0 to 6.5. During the experiments, a series of tip-speed-ratios were used to test the dynamic wind loads acting on the model wind turbine. It should be noted that a typical three blade HAWT in a modern wind farm usually has a tip-speed-ratio of $\lambda = 4.0$–8.0, as described in Burton et al. (2001).

In order to measure the dynamic wind loads acting on the model wind turbine, an aluminum rod was used as the turbine tower to support the nacelle and the rotor blades of the wind turbine model. Through a hole on the wind tunnel floor, the aluminum rod was connected to a high-sensitivity force-moment transducer (JR3, model 30E12A-I40) to measure the dynamic wind loads. The JR3 load cell is composed of foil strain gauge bridges, which are capable of measuring the forces on three orthogonal axes, and the moment about each axis. The precision of the force-moment sensor cell for the force measurements is $\pm 0.25\%$ of the full range 40 N. Although the JR3 load cell can provide time-resolved measurements of all three components of the aerodynamic forces and the moment (torque) about each axis, only the measured thrust coefficient, C_T, and the bending moment, C_{My}, are presented in this study. The thrust coefficient (i.e., the force coefficient in the stream-wise direction) and bending moment coefficient (i.e., the moment coefficient in the span-wise direction) were calculated using the expressions $C_T = T/(0.5\rho {U_{Hub}}^2 \pi R^2)$ and $CM_y = M_y/(0.5\rho {U_{Hub}}^2 \pi R^2 H)$, respectively, where ρ is the air density. For each tested case, the wind load data were acquired for 120 s at a sampling rate of 1000 Hz. For the tip-speed-ratio of $\lambda = 6.0$, the thrust coefficient C_T is estimated to be 0.538 for the type-1 ABL wind, which is similar to those of wind turbine models used in previous wind-tunnel tests, as listed in Table 1.

In this study, the mean wind speeds at turbine hub height for the two types of ABL winds were all set to be approximately $U_{Hub} = 5.0$ m/s. The Reynolds number based on the rotor diameter (D) and the oncoming wind speed at the hub height (U_{Hub}) was approximately 9.0×10^4, which is significantly lower than that of a utility-scale wind turbine (i.e., $\mathrm{Re} > 1.2\times10^6$). While the Reynolds number of a wind turbine may have a significant effect on the aeromechanic performances of the wind turbine, the flow characteristics in the turbine wake would become almost independent of the Reynolds number when the Reynolds number of the model turbine is higher enough. Chamorro et al. (2011) found that, the fundamental flow statistics in the turbine wake have asymptotic behavior with the Reynolds number. While the independence of Reynolds number for mean velocity was found to be reached at a lower value of $\mathrm{Re}\approx4.8\times10^4$, the Reynolds number independence would reach at $\mathrm{Re}\approx9.3\times10^4$ for higher order characteristics (i.e., shear stress and turbulence intensity). As mentioned above, the corresponding Reynolds number of the present study is approximately 9.0×10^4, which is in the range of the required minimum Reynolds number to achieve independence of the turbine flow statistics.

3. Results and discussion

3.1. Effect of wind shear on mean wind loads

As described above, two typical ABL winds with different wind shear and turbulence intensity levels were simulated in the present study. Fig. 3 shows the measured mean thrust coefficient, C_T, and bending moment coefficient, C_{My}, as functions of the tip-speed-ratio with the model wind turbine placed in different ABL winds. The profiles of the mean thrust and bending moment coefficients both were found to increase gradually with the increasing tip-speed-ratio of the wind turbine model. Similar trends were also reported by Adaramola and Krogstad (2011) for the variations of the mean thrust coefficients of a model wind turbine as a function of the tip-speed-ratio.

As shown in Fig. 3, the magnitudes of the thrust and bending moment coefficients are strongly dependent on the incoming ABL wind. The mean wind load coefficients of the model wind turbine were found to be smaller when placed in the type-1 ABL wind at all of the tested tip-speed-ratios, in comparison with those with the type-2 ABL wind. the difference between the mean wind loads for the two compared types of the ABL winds was found to increase gradually with the increasing tip-speed-ratio of the model turbine. As described in Dimitrov et al. (2015), the average wind speed at the hub height, U_{Hub}, is usually considered to have the greatest impact on the statistical wind loads. The measurement results given in Fig. 3 reveal that, the wind shear can also significantly influence the mean wind loads acting on wind turbines. As shown in Fig. 2, for the

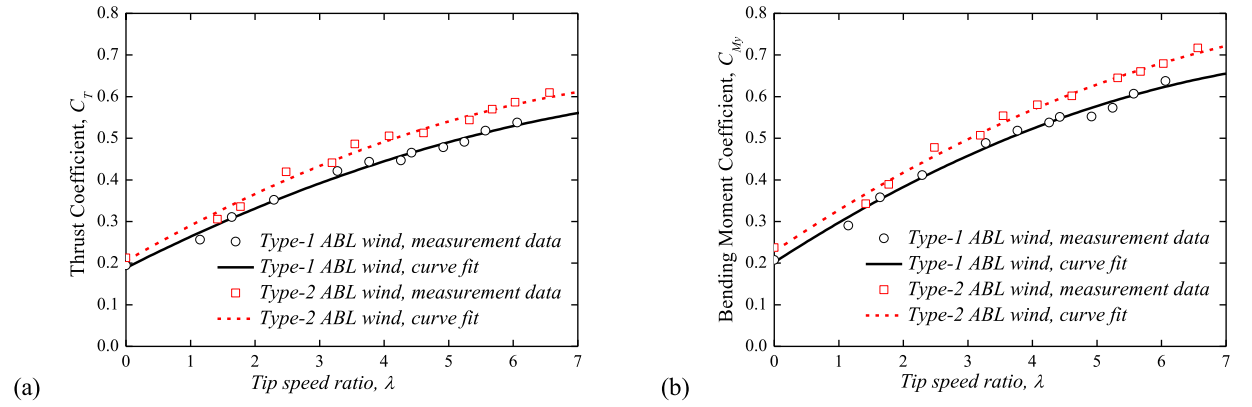

Fig. 3. Variations of the mean wind loads as functions of the tip-speed-ratio under different ABL winds. (a) Mean thrust coefficient; (b) mean bending moment coefficient.

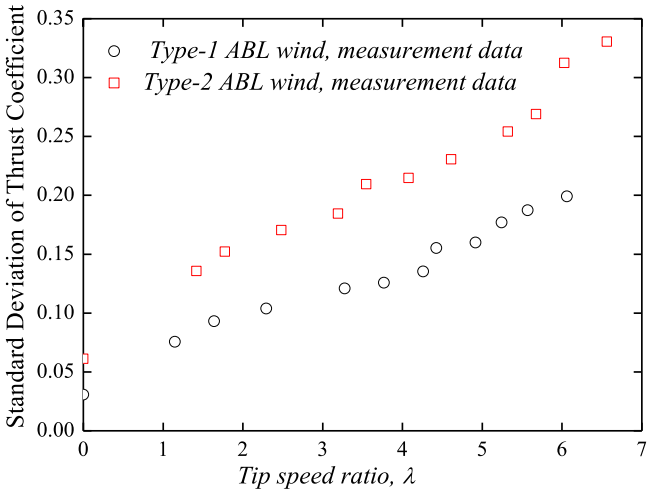

Fig. 4. Variations of the σ_{C_T} values as a function of the tip-speed-ratio under two different ABL winds.

type-2 ABL wind with a higher wind shear exponent (i.e., $\alpha = 0.16$), the relative mean wind speed U/U_{Hub} is higher in the region above the hub height. Due to the effects of the tower and ground (i.e., the speed of the incoming ABL wind is much lower in the region near the ground), the rotor in the region above the hub height would harvest much more wind energy from the incoming flow and experience higher wind loads than those in the region below the hub height. Therefore, the high relative wind speed U/U_{Hub} above the hub height is believed to contribute to the higher mean wind loads for the type-2 ABL wind, as shown in Fig. 3.

3.2. Effects of turbulence intensity of the incoming airflow on fatigue loads

As described by Dekker and Pierik (1998), the fatigue damage to a wind turbine is closely related to the turbulence characteristics of the wind field, such as turbulence intensity, length scale and coherence, of which the turbulence intensity is by far the most significant. Fig. 4 shows the standard deviation of the dynamic thrust coefficient, σ_{C_T}, as functions of the tip-speed-ratio of wind turbines when placed in two different types of ABL winds. The σ_{C_T} values were found to increase gradually with the increasing tip-speed-ratio, which is similar as the trends of the mean wind load data shown in Fig. 3. In addition, it can also be seen clearly that, in comparison to the mean thrust coefficients, the difference of the σ_{C_T} values between the two compared types of ABL winds are much more significant, which indicates the more significant effects of the turbulence intensity level of the incoming ABL wind on the fatigue loads acting on wind turbines. Due to the much lower turbulence level in the incoming airflow, the wind turbine sited in the type-1 ABL wind was found to experience much lower fatigue loads, in comparison to that when sited in the type-2 ABL wind.

Besides the standard deviation values of the thrust coefficients, the time histories of the instantaneous thrust forces acting on the model wind turbine at a typical tip-speed-ratio of $\lambda = 6.0$ were selected to further evaluate the effects of inflow

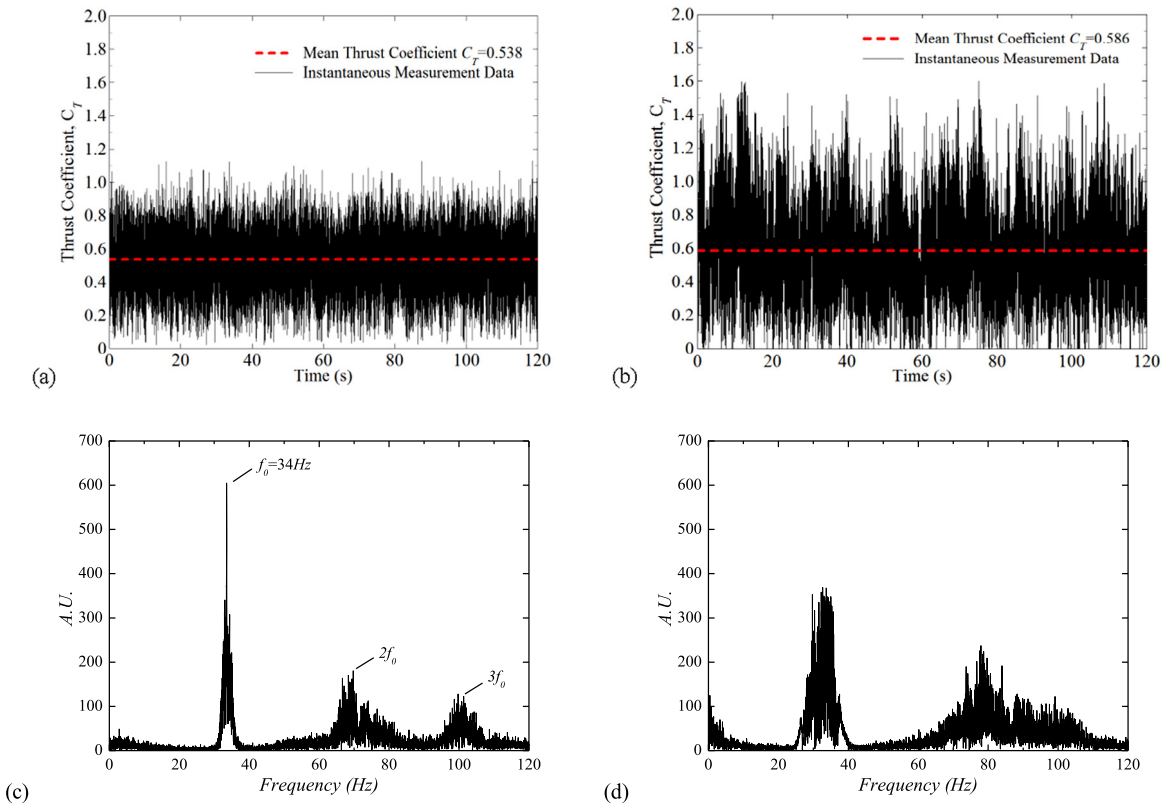

Fig. 5. Measured dynamic wind loads acting on the wind turbine model. (a) Time history of C_T in type-1 ABL wind; (b) time history of C_T in type-2 ABL wind; (c) power spectrum of C_T, in type-1 ABL wind; (d) power spectrum of C_T, in type-2 ABL wind.

turbulence level on the behaviors of the dynamic wind loads. The time histories of the instantaneous thrust force acting on the model wind turbine sited in the two compared ABL winds with different turbulence intensity levels are shown in Fig. 5(a) and (b). The mean values are also plotted as dashed lines in the plots for comparison. The extreme wind loads acting on the wind turbine were found to be approximately 2–3 times higher than the mean values. Jiang et al. (2015) reported similar behaviors of the dynamic wind loads by measuring the time series of the radial contact force of the National Renewable Energy Laboratory's (NREL) 750 kW wind turbine planetary bearing. In addition, as shown clearly in Fig. 5(a) and (b), the differences between the fluctuation amplitudes of the instantaneous and the extreme wind loads under the two compared ABL winds were found to be much greater than those in the measured mean wind loads. The extreme thrust coefficient of the model wind turbine was found to reach as high as $C_T = 1.6$ when sited in the type-2 ABL wind, which is approximately 45% greater than the corresponding value when sited in the type-1 ABL wind (i.e., $C_T = 1.1$).

Fig. 5(c) and (d) show the power spectra of the measured instantaneous thrusts obtained using a fast Fourier transform (FFT) analysis procedure. A dominant peak at $f_0 = 34$ Hz can be identified clearly in the spectrum given in Fig. 5(c), corresponding to the rotational speed of the turbine rotor blades at the tip-speed-ratio of $\lambda = 6.0$. This rotational frequency agrees well with the value measured independently using a tachometer (Monarch Instrument). Other peaks, which represent the harmonic frequencies of the turbine rotation frequency, f_0, can also be identified clearly from the power spectrum plots. However, no dominant peak can be identified in the spectrum for the test case with high turbulent incoming ABL wind, as shown in Fig. 5(d). The rotational speed of the turbine rotor blades was found to fluctuate in a wide range of frequencies (i.e., 28 Hz $< f_0 <$ 36 Hz). The harmonic frequencies of the rotational frequency of the turbine, especially for $3f_o$, are very difficult to identify in the plot, in comparison to the scenario with lower turbulence levels in the incoming ABL wind. These significant fluctuations in the rotational speed of the turbine rotor blades would cause much greater variations of the dynamic wind loads, therefore, higher fatigue loads acting on the wind turbine when sited in the type-2 ABL wind, due to the nearly two times higher in the turbulence intensity of the incoming ABL wind.

Fig. 6(a) and (b) show histograms of the measured dynamic thrust that acts on the wind turbine model. Whereas the instantaneous wind loads on the wind turbine model were found to be highly unsteady with randomly fluctuating magnitudes, the histograms of the measured thrust coefficients for both the low and high turbulence ABL winds were fit well by Gaussian functions, which confirms that it is reasonable to use the standard deviation values of the dynamic wind loads to estimate the fatigue loads on the wind turbine. The standard deviation values of the thrust coefficient for the model wind turbine in the low turbulence wind environment was found to be 0.20, and the corresponding value in the high turbulence

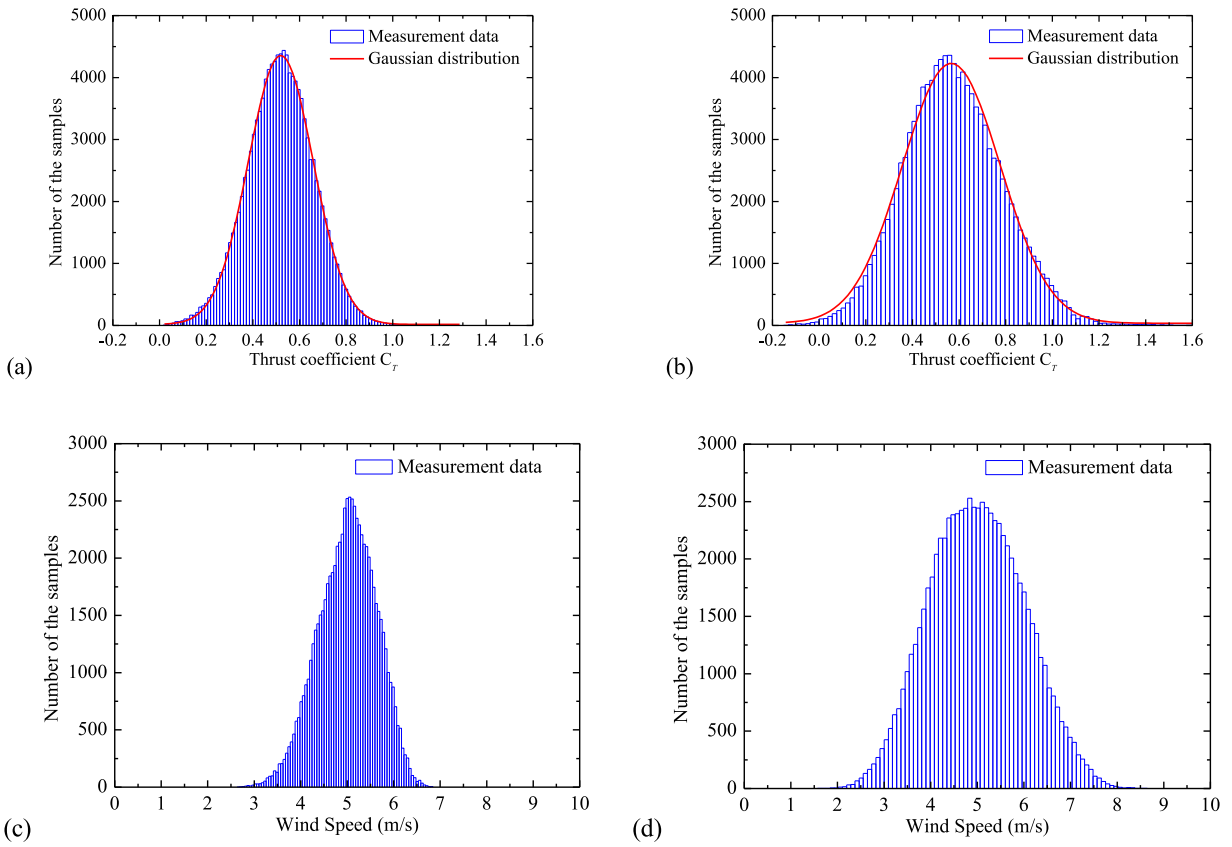

Fig. 6. Histogram of instantaneous thrust coefficients and hub height wind speeds. (a) histogram of C_T in type-1 ABL wind; (b) histogram of C_T in type-2 ABL wind; (c) histogram of hub height wind speed in type-1 ABL wind; (d) histogram of hub height wind speed in type-2 ABL wind.

wind environment was 0.31. The larger standard deviation value indicates that much more severe fatigue loads would act on the wind turbines when operated in the high turbulence wind environment.

The behavior of dynamic wind loads acting on the model wind turbine was found to be highly related to the local flow characteristics. The histograms of the instantaneous inflow velocity measured at turbine hub height are plotted in Fig. 6(c) and (d). While the mean wind speeds at the turbine hub height were set to be the same, the histogram distributions of the instantaneous wind speeds of the two compared incoming ABL winds show significant difference due to the different turbulence intensity levels. It can be seen clearly that, the instantaneous wind speeds for the type-2 ABL wind varied in a much wider range. Therefore, the model wind turbine sited in type-2 ABL wind would have a much higher chance to experience instantaneous wind speeds far from the mean value, which could be the reason for the higher fatigue loads acting on the model wind turbine when placed in high turbulence wind environment.

3.3. Dynamic wind loads acting on different components of the wind turbine model

In the present study, the wind turbine model can be disassembled into three parts: tower, nacelle and rotor. Fig. 7 shows the mean and fatigue thrust coefficients that act on each of the three components of the wind turbine model when placed in the type-1 and type-2 ABL winds. The rotating case corresponds to the wind turbine operating at the typical tip-speed-ratio of $\lambda = 6.0$, and the results for the stationary case refer to the wind loads when the rotor of the wind turbine is not in rotation. The effects of the wind shear on the mean wind loads of the different components of the wind turbine model are shown clearly in Fig. 7(a). It should be noted that, while the mean wind speed at the turbine hub height was set to $U_{Hub} = 5.0$ m/s for both the type-1 and type-2 ABL winds, the wind speed of the type-2 ABL wind case (i.e., having a power law exponent of $\alpha = 0.16$) is lower in the region below the hub height than that of the type-1 ABL wind (i.e., having a power law exponent of $\alpha = 0.11$). This results in lower mean forces acting on the turbine tower and nacelle when placed in the type-2 ABL wind. After adding the rotor, the mean forces that act on the stationary and rotating wind turbines become higher for the case in type-2 ABL wind. The reason for this experimental observation, in which the mean wind loads reverse after adding the rotor, has been explained in Section 3.1.

Without the rotor, the wind loads that act on the turbine tower and nacelle together contribute only approximately 10% of the total wind loads (i.e., the test case with the wind turbine rotating at the tip-speed-ratio of $\lambda = 6.0$). It indicates that

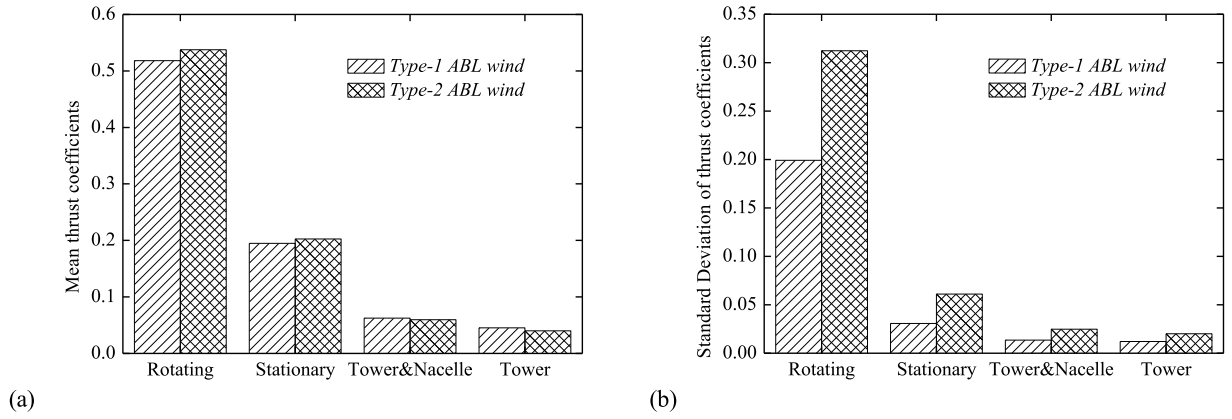

Fig. 7. Comparison of the dynamic thrusts that act on different components of the wind turbine model. (a) mean thrust coefficients; (b) standard deviations of the thrust coefficients.

approximately 90% of the wind loads acting on the model wind turbine in rotation was found to come from the rotating rotor. The quantitative measurement results highlight the importance of the mechanical design of the connecting parts between the rotor and nacelle (i.e., the shaft and gear system). In addition, wind turbines are controlled to stop to prevent damage when the wind exceeds the "cut-out" speed (i.e., >25 m/s). However, as shown in Fig. 7(a), the mean wind loads acting on a stationary wind turbine can reach approximately 38% of the wind loads on a rotating wind turbine. Thus, the wind loads that act on a wind turbine under extreme wind conditions still need to be considered properly even though the turbine was shut down (i.e., the rotor is stopped from rotation).

As described in Section 3.2, the standard deviation values of the measured wind loads can be used to represent the fatigue loads for the test cases with both low and high turbulence ABL winds. As shown in Fig. 7(b), the fatigue loads acting on the tower and nacelle together were found to be less than 8% of the total fatigue loads on a rotating wind turbine. It indicates that, more than 92% of the fatigue loads would come from the rotating rotor, the value was found to be even greater than the proportion of the mean wind loads of the rotating rotor. Moreover, the fatigue loads acting on the stationary wind turbine (i.e., in "shut-down" mode) represent 15%–20% of the total fatigue loads acting on the rotating wind turbine. In contrast, the contribution of the stationary wind turbine (i.e., turbine in "shut-down" mode) to the mean wind loads was found to be approximately 38%. Thus, in comparison to the fatigue loads, the mean wind loads acting on a wind turbine under extreme wind conditions must be considered carefully. It should also be noted that, the turbulence intensity levels in ABL winds was found to play a dominant role in determining the characteristics of the fatigue loads acting on different components of the wind turbine. As shown clearly in Fig. 7, in comparison with those in type-1 ABL wind, even though the mean wind loads acting on the turbine tower and nacelle were found to be smaller in type-2 ABL wind, the fatigue loads were found to be much higher corresponding to the high ambient turbulence intensity in type-2 ABL wind.

3.4. Dynamic wind loads on stationary wind turbine model with the rotor blades in different phase angles

As described above, the mean wind loads acting on the stationary wind turbine (i.e., in "shut-down" mode) can be as high as 38% of those of the wind turbine rotating at a tip-speed-ratio of $\lambda = 6.0$. For an offshore wind farm, extreme wind conditions (i.e., >25 m/s) may occur quite often. Thus, it is important to reduce the wind loads acting on stationary wind turbines (i.e., turbine in "shut-down" mode). Fig. 8 shows the dynamic wind loads of the wind turbine in "shut-down" mode under type-1 ABL wind and the turbine rotor blades were set in different phase angles. In the present study, the phase angle of the rotor blades was defined as the angle between the vertical plane through the rotational axis of the wind turbine model and the position of a pre-marked rotor blade.

Fig. 8(a) shows the variations of the mean wind loads acting on the wind turbine in "shut-down" mode as a function of the phase angles of the rotor blades. The mean wind loads were found to decrease with the increasing phase angle at first, reaching a minimum value at the phase angle of $\theta = 60°$, and then increase with further increase in the phase angle. It can be seen that, the configuration with one of the blades being in front of the tower, i.e., at the phase angle of $\theta = 60°$, can significantly decrease the wind loads acting on the turbine tower. Moreover, the top tip height reached by the wind turbine blades would be the lowest at the phase angle of $\theta = 60°$, thus, the rotor would experience lower wind speeds in the ABL wind, in comparison to those at the other phase angles. Therefore, the mean wind loads were found to be the minimum at the phase angle of $\theta = 60°$. As shown in Fig. 8(a), the mean thrust and bending moment coefficients at $\theta = 60°$ were found to be $C_T = 0.165$ and $CM_y = 0.177$, respectively, which were approximately 15% less than the maximum loads that occurred at $\theta = 0°$. Therefore, the mean wind loads acting on the stationary wind turbine (i.e., turbine in "shut-down" mode) can be reduced by adjusting the turbine blades to an appropriate phase angle. Furthermore, Fig. 8(b) shows that the variations of the fatigue loads with the phase angle follow the same trend as the variations in the mean wind loads. The minimum fatigue

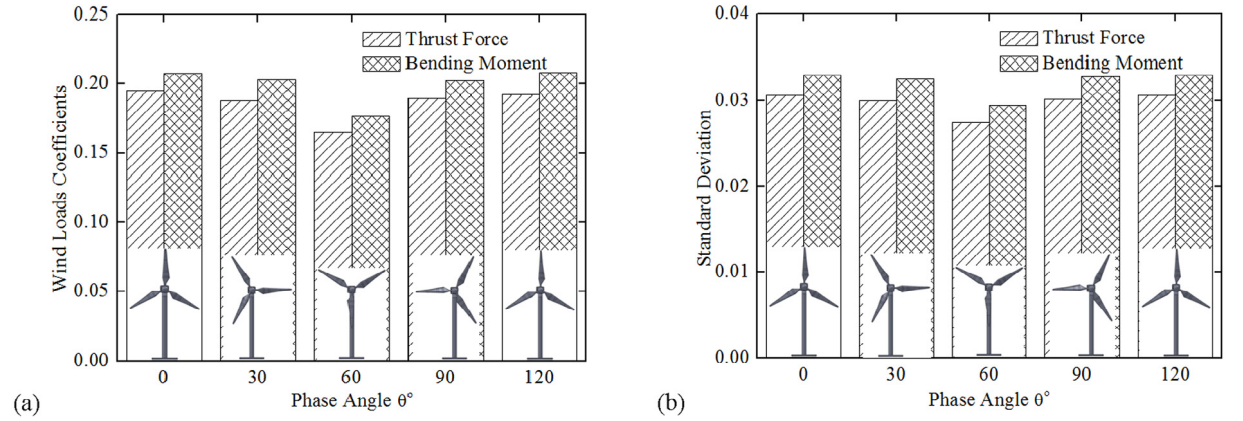

Fig. 8. Dynamic wind loads that act on the stationary wind turbine with different blade phase angles. (a) mean wind loads; (b) fatigue wind loads.

loads were also found to occur at the phase angle of $\theta = 60°$, and were 10% lower than the maximum fatigue loads occurred at of $\theta = 0°$.

4. Conclusion

A comprehensive experimental study was conducted in an atmospheric boundary layer (ABL) wind tunnel to analyze the characteristics of the dynamic wind loads acting on a typical three-blade horizontal axial wind turbine model. Two types of ABL winds were simulated to study the effects of the wind shear and the turbulence intensity of the incoming ABL wind on the dynamic wind loads acting on the wind turbine model. While the average wind speed at the hub height U_{Hub} is usually recognized as having the greatest effects on the wind load characteristics, the wind shear was also found to significantly influence the mean wind loads acting the wind turbine. The ABL wind with greater wind shear will lead to higher mean wind loads acting on the wind turbine. The higher turbulence level in the incoming ABL wind was found to result in significant fluctuations in the rotational speed of the turbine rotor blades, leading to much greater variations of the dynamic wind loads, therefore, higher fatigue loads on the wind turbine.

The dynamic wind loads acting on different components of the wind turbine model were also identified in the present study. The experimental results highlight the role of the rotating rotor, which was found to contribute more than 90% both in the mean and fatigue wind loads acting on a wind turbine. In addition, the mean wind loads acting on the stationary wind turbine (i.e., turbine in "shut-down" mode) can reach approximately 38% of those acting on a rotating wind turbine, suggesting that the wind loads acting on a wind turbine under extreme wind conditions must be considered properly even though the wind turbine was set in "shut-down" mode.

In order to reduce damages to wind turbines under extreme wind conditions, an experimental study was also conducted to evaluate the variations of the wind loads acting on a stationary wind turbine (i.e., in "shut-down" mode) as a function of the phase angles of the rotor blades. The stationary wind turbine was found to experience the lowest wind loads at the phase angle of $\theta = 60°$ i.e., the configuration with one of the blades being in front of the tower. The maximum variation between the different blade phase angles was found to reach 15% for the mean wind loads and 10% for the fatigue loads acting on the wind turbine in "shut-down" mode.

It should be noted that, wind tunnel experiments were usually preformed with simplified inflow conditions and scaled wind turbine models, which is different from the scenario of utility-scale wind turbine operating under realistic ABL conditions. Instead, numerical simulation could be an effective approach to study utility-scale wind turbines operating under realistic ABL flow conditions (Bhaganagar and Debnath, 2015). However, because the atmospheric flow of field tests is difficult to describe in sufficient detail due to its complicated characteristics (De Vries, 1983), it is rarely possible to use field test to get all of the information needed for a well-defined test case for numerical simulations. The wind-tunnel results obtained in the present study for scaled wind turbine model is essential due to its ability of producing well-controlled flow conditions, which can provide sufficient information for the validation and verification of the numerical simulations.

Acknowledgments

Funding support from the Iowa Alliance for Wind Innovation and Novel Development (IAWIND), USA and National Science Foundation (NSF), USA with Grant No. CBET-1133751 and CBET-1438099 is gratefully acknowledged. Wei Tian also wants to thank the support from the Shanghai Natural Science Foundation, China (No. 16ZR1417600) and National Key Technology Support Program of China (No. 2015BAA06B04).

References

Abdallah, I., Natarajan, A., Sørensen, J.D., 2016. Influence of the control system on wind turbine loads during power production in extreme turbulence: Structural reliability. Renew. Energy 87, 464–477.

Adaramola, M., Krogstad, P., 2011. Experimental investigation of wake effects on wind turbine performance. Renew. Energy 36, 2078–2086.

Alfredsson, P.H., Dahlberg, J.A., Vermeulen, P.E.J., 1982. A comparison between predicted and measured data from wind turbine wakes. Wind Eng. 6, 149–155.

Architecture Institute of Japan, 1996. AIJ Recommendations for Loads on Buildings. Publisher: Architectural Institute of Japan, ISBN: 978-4-81-890459-0.

Bak, C., Zahle, F., Bitsche, R., Kim, T., Yde, A., Henriksen, L.C., Natarajan, A., Hansen, M., 2013. Description of the DTU 10 MW reference wind turbine. DTU Wind Energy Report-I-0092.

Barthelmie, R., Hansen, O., Enevoldsen, K., Højstrup, J., Larsen, S., Frandsen, S., Pryor, S., Motta, M., Sanderhoff, P., 2005. Ten years of meteorological measurements for offshore wind farms. J. Solar Energy Eng. 127, 170–176.

Bhaganagar, K., Debnath, M., 2015. The effects of mean atmospheric forcings of the stable atmospheric boundary layer on wind turbine wake. J. Renew. Sustain. Energy 7, 58–87.

Burton, T., Sharpe, D., Jenkins, N., Bossanyi, E., 2001. Wind Energy Handbook. John Wiley & Sons Ltd, England.

Cal, R.B., Lebron, J., Castillo, L., Kang, H.S., Meneveau, C., 2010. Experimental study of the horizontally averaged flow structure in a model wind-turbine array boundary layer. J. Renew. Sustain. Energy 2, 013106.

Chamorro, L.P., Arndt, R.E.A., Sotiropoulos, F., 2011. Reynolds number dependence of turbulence statistics in the wake of wind turbines. Wind Energy 15, 733–742.

De Vries, O., 1983. On the theory of the horizontal-axis wind turbine. Ann. Rev. Fluid Mech. 15, 77–96.

Dekker, J.W.M., Pierik, J.T.G., 1998. European wind turbine standards. II. Project results. ECN-C-99-073.

Dimitrov, N., 2015. Comparative analysis of methods for modelling the short-term probability distribution of extreme wind turbine loads. Wind Energy 19, 717–737.

Dimitrov, N., Natarajan, A., Kelly, M., 2015. Model of wind shear conditional on turbulence and its impact on wind turbine loads. Wind Energy 18, 1917–1931.

Dimitrov, N., Natarajan, A., Mann, J., 2017. Effects of normal and extreme turbulence spectral parameters on wind turbine loads. Renew. Energy 101, 1180–1193.

Grant, I., Parkin, P., Wang, X., 1997. Optical vortex tracking studies of a horizontal axis wind turbine in yaw using laser-sheet, flow visualization. Exp. Fluids 23, 513–519.

Haans, W., Sant, T., van Kuik, G., van Bussel, G., 2008. HAWT near-wake aerodynamics, part I: axial flow conditions. Wind Energy 11, 245–264.

Hancock, P.E., Pascheke, F., 2010. Wind tunnel simulations of wind turbine wake interactions in neutral and stratified wind flow. In: 10th EMS Annual Meeting, 10th European Conference on Applications of Meteorology (ECAM). Zurich, Switzerland.

Hansen, K.S., Barthelmie, R.J., Jensen, L.E., Sommer, A., 2012. The impact of turbulence intensity and atmospheric stability on power deficits due to wind turbine wakes at Horns Rev wind farm. Wind Energy 15, 183–196.

Hu, H., Yang, Z., Sarkar, P., 2012. Dynamic wind loads and wake characteristics of a wind turbine model in an atmospheric boundary layer wind. Exp. Fluids 52, 1277–1294.

IEC, 2005. International Standard IEC 61400-1: Wind Turbines—Part 1: Design Guidelines.

Jiang, Z., Xing, Y., Guo, Y., Moan, T., Gao, Z., 2015. Long-term contact fatigue analysis of a planetary bearing in a land-based wind turbine drivetrain. Wind Energy 18, 591–611.

Larsen, T.J., Madsen, H.A., Larsen, G., Hansen, K.S., 2013. Validation of the dynamic wake meander model for loads and power production in the Egmond aan Zee wind farm. Wind Energy 16, 605–624.

Lee, S., Churchfield, M., Moriarty, P., Jonkman, J., Michalakes, J., 2011. Atmospheric and wake turbulence impacts on wind turbine fatigue loading. National Renewable Energy Laboratory, Technical Report No. NREL/CP-5000-53567.

Locke, J., Valencia, U., 2004. Design studies for twist-coupled wind turbine blades. Sandia National Laboratories, Technical Report No. SAND 2004–0522.

Medici, D., Alfredsson, P., 2006. Measurements on a wind turbine wake: 3D effects and bluff body vortex shedding. Wind Energy 9, 219–236.

Moriarty, P.J., Holley, W.E., Butterfield, S.P., 2004. Extrapolation of extreme and fatigue loads using probabilistic methods, National Renewable Energy Laboratory, Technical Report No. NREL/TP-500-34421.

Nguyen, H.H., Manuel, L., 2015. A Monte Carlo simulation study of wind turbine loads in thunderstorm downbursts. Wind Energy 18, 925–940.

Riziotis, V.A., Voutsinas, S.G., 2000. Fatigue loads on wind turbines of different control strategies operating in complex terrain. J. Wind Eng. Ind. Aerodyn. 85, 211–240.

Sathe, A., Mann, J., Barlas, T., Bierbooms, W.A.A.M., van Bussel, G.J.W., 2013. Influence of atmospheric stability on wind turbine loads. Wind Energy 16, 1013–1032.

Smith, C.M., Barthelmie, R.J., Pryor, S.C., 2013. In situ observations of the influence of a large onshore wind farm on near-surface temperature, turbulence intensity and wind speed profiles. Environ. Res. Lett. 8, 34006.

Somers, D.M., 2005. The S819, S820, and S821 airfoils. National Renewable Energy Laboratory, Technical Report No. NREL/SR-500-36334.

Tian, W., Ozbay, A., Hu, H., 2014a. An experimental investigation on dynamic wind loads acting on a wind turbine model in atmospheric boundary layer winds. In: 32nd ASME Wind Energy Symposium, National Harbor. Maryland.

Tian, W., Ozbay, A., Hu, H., 2014b. Effects of incoming surface wind conditions on the wake characteristics and dynamic wind loads acting on a wind turbine model. Phys. Fluids 26, 125108.

Vermeer, L.J., Sørensen, J.N., Crespo, A., 2003. Wind turbine wake aerodynamics. Prog. Aerosp. Sci. 39, 467–510.

Whale, J., Anderson, C., Bareiss, R., Wagner, S., 2000. An experimental and numerical study of the vortex structure in the wake of a wind turbine. J. Wind Eng. Ind. Aerodyn. 84, 1–21.

Wilson, R.E., 1994. Aerodynamic behavior of wind turbines. In: Spera, DA (Ed.), Wind Turbine Technology: Fundamental Concepts of Wind Turbine Engineering. ASME Press, pp. 215–282.

Yoshida, S., Goltenbott, U., Ohya, Y., Jamieson, P., 2016. Coherence effects on the power and tower loads of a $7\times$ 2 MW multi-rotor wind turbine system. Energies 9, 742.

Yuan, W., Tian, W., Ozbay, A., Hu, H., 2014. An experimental study on the effects of relative rotation direction on the wake interferences among tandem wind turbines. Sci. China Phys. Mech. Astron. 57, 935–949.

Zhang, W., Markfort, C.D., Porte-Agel, F., 2012. Near-wake flow structure downwind of a wind turbine in a turbulent boundary layer. Exp. Fluids 52, 1219–1235.

Zhang, Y., Sarkar, P.P., Hu, H., 2015. An experimental investigation on the characteristics of fluid–structure interactions of a wind turbine model sited in microburst-like winds. J. Fluids Struct. 57, 206–218.

Zhou, Y., Kareem, A., 2002. Definition of wind profiles in ASCE 7. J. Struct. Eng. 128, 1082–1086.